



Geophysical Research Letters

RESEARCH LETTER

10.1029/2020GL090288

Key Points:

- The atmospheric responses to winter sea ice decline are examined by dividing sea ice decline events into upward and downward anomalous surface turbulent heat flux (ASTHF) events
- The upward ASTHF events could potentially have a large impact on the overlying atmosphere. The downward ASTHF events show opposite features
- On the intraseasonal time scale, caution is called for when designing model experiments using observed sea ice decline

Supporting Information:

Supporting Information may be found in the online version of this article.

Correspondence to:

Z. Jiang, jiangzn@cma.gov.cn

Citation:

Jiang, Z., Feldstein, S. B., & Lee, S. (2021). Two atmospheric responses to winter sea ice decline over the Barents-Kara Seas. *Geophysical Research Letters*, 48, e2020GL090288. https://doi.org/10.1029/2020GL090288

Received 16 AUG 2020 Accepted 6 JAN 2021

© 2021. American Geophysical Union. All Rights Reserved.

Two Atmospheric Responses to Winter Sea Ice Decline Over the Barents-Kara Seas

Zhina Jiang¹, Steven B. Feldstein², and Sukyoung Lee²

¹State Key Laboratory of Severe Weather (LaSW), Chinese Academy of Meteorological Sciences, Beijing, China, ²Department of Meteorology and Atmospheric Science, The Pennsylvania State University, University Park, PA, USA

Abstract The intraseasonal atmospheric responses to winter sea ice decline over the Barents-Kara Seas are examined by dividing rapid sea ice decline events into two categories, based on the direction (upward vs. downward) of the anomalous surface turbulent heat flux (ASTHF) after the sea ice loss. The upward ASTHF events, which could potentially have a large impact on the overlying atmosphere, are characterized by anomalously negative total column water and surface air temperature minus skin temperature, and anomalously positive surface wind speed following the sea ice loss. The downward ASTHF events show opposite features. Both types of events are linked to the Madden-Julian Oscillation and subsequent circulation anomalies. This result indicates that on the intraseasonal time scale, not all sea ice decline events influence the atmosphere, and caution is called for when designing transient model experiments using observed sea ice decline.

Plain Language Summary Wintertime Arctic sea ice has undergone a rapid decline during the past few decades. The question of whether sea ice decline has an influence on the atmosphere is explored at intraseasonal time scales during the winter season by dividing rapid sea ice decline events into two categories based on the direction (upward vs. downward) of the anomalous surface turbulent heat flux (ASTHF) over the Barents-Kara Seas after sea ice loss. Only the upward ASTHF events have the potential to have a large impact on the atmosphere. This difference in the direction of the ASTHF after the sea ice loss is found to be linked to different properties of surface air temperature, skin temperature, moisture and wind speed over the BKS for the two types of events. Furthermore, it is found that the direction of the ASTHF is also related to the tropical Madden-Julian Oscillation and wind anomalies that follow. Modeling studies often employ observed/simulated sea ice loss as a boundary forcing to evaluate their impact on the atmosphere. The result of this study can be used to refine such a modeling approach.

1. Introduction

There has been a large body of literature that investigates whether a large seasonal-mean and interannual decline in Arctic sea ice can have a marked impact on the atmosphere (e.g., Backport et al., 2019; Deser et al., 2004; Honda et al., 2009; Inoue et al., 2012; Kug et al., 2015; Liptak & Strong, 2014; Magnusdottir et al., 2014; Peings & Magnusdottir, 2014; Perlwitz et al., 2015; Petoukhov & Semenov, 2010; Rigor et al., 2002; Rinke et al., 2006; Screen et al., 2012; Sorokina et al., 2016). Other studies have examined whether the atmosphere has played an important role in driving seasonal-mean and interannual sea ice declines (e.g., Blackport et al., 2019; Francis & Hunter, 2006; Sorteberg & Kvingedal, 2006). The same question is addressed as to whether intraseasonal sea ice loss has had a large impact on the atmosphere (e.g., Deser et al., 2007; Honda et al., 1999; Gong et al., 2020), and vice versa (e.g., B. H. Luo et al., 2017, 2019; Blackport et al., 2019; Chen et al., 2018; Fang & Wallace, 1994; Gong & Luo, 2017; D. H. Luo et al., 2016a, 2016b; D-S. R. Park et al., 2015; H-S. Park, Lee, Kosaka, et al., 2015; Tyrlis et al., 2020; Woods & Caballero, 2016; Zhong et al., 2018).

In a recent study, Blackport et al. (2019) examined the two-way interaction between the atmosphere and sea ice when the sea ice concentration (SIC) is anomalously low over the Barents-Kara Seas (BKS) and the Chukchi and Bering Seas. They found that about half of reduced SIC seasons/months are characterized by a downward surface turbulent heat flux (STHF, surface sensible heat flux plus surface latent heat flux) anomaly, and the other remaining seasons/months are dominated by an upward STHF anomaly.

JIANG ET AL.



The question of whether the anomalous STHF (ASTHF) is upward or downward after the loss of sea ice is important. If the ASTHF is upward, there is the potential for the sea ice loss to have a large impact on the atmosphere because Rossby waves can be excited which propagate vertically and equatorward into midlatitudes (e.g., Alexander et al., 2004; Deser et al., 2004; Honda et al., 2009; Rinke et al., 2006). However, if the ASTHF is downward, the reduced sea ice has minimal influence on the atmosphere (Blackport et al., 2019; Gong et al., 2020).

Several recent papers have found this two-way interaction between the atmosphere and sea ice in daily data. In these papers, most of the sea ice decline takes place over a time period of 1 week. The overall picture from studies such as D-S. R. Park et al. 2015, H-S. Park, Lee, Son, et al. (2015), Lee et al. (2017), Gong et al. (2017), and Woods and Caballero (2016) is that the melting of BKS sea ice is preceded several days earlier by the intrusion of warm, moist air from the midlatitudes into the Arctic, and an increase in the downward infrared radiation (DIR) at the surface and a downward ASTHF. These studies found that the increase in surface DIR is the main driver of the sea ice melting, but that wind-driven sea ice motion also plays an important role (D-S. R. Park et al., 2015; H-S. Park, Lee, Son, et al., 2015). After the ocean surface is exposed, they found upward STHF and DIR anomalies.

Gong and Luo (2017), B. H. Luo et al. (2017, 2019), Chen et al. (2018), and Tyrlis et al. (2020) examined the impact of Ural blocking on BKS sea ice loss. The general picture from these studies matches those mentioned above. In one particular study (Chen et al., 2018), in which Ural blocks with different longitudes were examined, it was found that the ASTHF is always downward prior to the melting of the sea ice, but that the ASTHF either switches to being upward or remained downward following the reduction in sea ice, depending upon the longitude of the block.

In this study, we address the question of what factors determine the direction of the ASTHF after the sea ice decline by examining the *daily variation* of the ASTHF. Selecting from the top and bottom bins of the probability density function of the ASTHF, one category is characterized by an upward ASTHF following the sea ice decline and the other category by a downward ASTHF.

2. Data and Method

The daily (0000 UTC) ERA-Interim reanalysis data set of the European Center for Medium-Range Weather Forecasts (ECMWF) is used for the years 1979–2017 (Dee et al., 2011). The variables examined here include Arctic SIC with a 1.0° × 1.0° latitude/longitude resolution, and surface air temperature (SAT), skin temperature (SKT), sea level pressure (SLP), 10-m wind speed (V10 m), 500-hPa geopotential height (GP500), 300-hPa streamfunction, total column water (TCW), surface downward IR (DIR), vertical integral of moisture flux and moisture flux divergence (MFD), and the surface sensible and latent heat flux (SSHF and SLHF), with a 2.5° × 2.5° latitude/longitude spatial resolution. For the forecasted variables, such as DIR, SSHF and SLHF, the difference between the daily accumulated values at time steps 6 and 3 for 0000 UTC is calculated, and then divided by the time interval in seconds to find the values for that day. As shown by D-S. R. Park et al. (2015), the ERA-Interim SIC data show good agreement with the SIC data from the National Snow and Ice Data Center (NSIDC; Cavalieri et al., 1996). However, NSIDC SIC data are available every two days from the year 1979 to 1989, and then daily starting 1990. Because the daily variation of SIC needs to be examined in this study, ERA-Interim SIC data are used. We also use the NSIDC daily 25-km EASE-Grid sea ice motion data set (Tschudi et al., 2019) and sea-ice thickness data from the coupled Pan-Arctic Ice Ocean Modeling and Assimilation System (PIOMAS; Zhang & Rothrock, 2003).

Anomalies of variables are calculated by subtracting the seasonal cycle at each grid point, where the seasonal cycle is represented by the first four harmonics of the calendar-day mean annual cycle. For each of the above variables (SAT, SKT, TCW, DIR, MFD, STHF, SSHF, and SLHF), indices are defined by averaging the corresponding anomalies weighted by cosine (latitude) over the BKS $(30^{\circ}-70^{\circ}E, 70^{\circ}-80^{\circ}N)$ (Kug et al., 2015). Some of the variables are standardized, as indicated in the corresponding figure caption. (The standard deviations of each variable are listed in the supplementary section as Table S1.) To test the sensitivity of our results to the boundaries of the BKS domain, calculations are performed for the domain of $(30^{\circ}-90^{\circ}E, 65^{\circ}-80^{\circ}N)$. The results are very similar to those presented in this study, and our conclusions remain unchanged.

JIANG ET AL. 2 of 10



In order to identify sea ice decline events, we use a daily SIC tendency index, which is based on the forward difference of the daily SIC anomaly averaged over the BKS between two adjacent days. A sea ice decline event is identified if the SIC tendency index exceeds -1.0 standard deviation for at least three consecutive days. If the beginning of an event occurs within 4 days of the end of the preceding one, then the latter event is discarded. This analysis is limited to events that take place within the winter period, that is December–February (DJF), although a few days in November and March are included for compositing days that occur either before, or after, an event, respectively. During the 39 boreal winters of 1979–2017, 64 rapid sea ice decline events are identified. Lag zero is defined as the onset day of sea ice decline, where onset day is defined as the first day when the SIC tendency index exceeds the above threshold value. (The start date and duration for these events are listed in Table S2 of the supplementary section.) For the composite calculations, Monte Carlo bootstrapping, as in Jiang et al. (2017), and *Student's-t* tests are used to evaluate the statistical significance.

3. Results

3.1. Characteristics of Selected Meteorological Variables During Rapid Sea Ice Decline Events

We first examine the temporal relationship between SIC and ASTHF for the rapid sea ice decline events. As can be seen in Figure 1a, the upward ASTHF is strongest at lag +11 days, 10 days after the maximum SIC tendency, which is consistent with previous studies (D-S. R. Park et al., 2015). (Note that the ECMWF sign convention for STHF is that positive [negative] values indicate a downward [upward] STHF.) The anomalous BKS sea ice remains negative until lag +30 days (the total SIC decline from lag 0 to lag +7 days is approximately 15%).

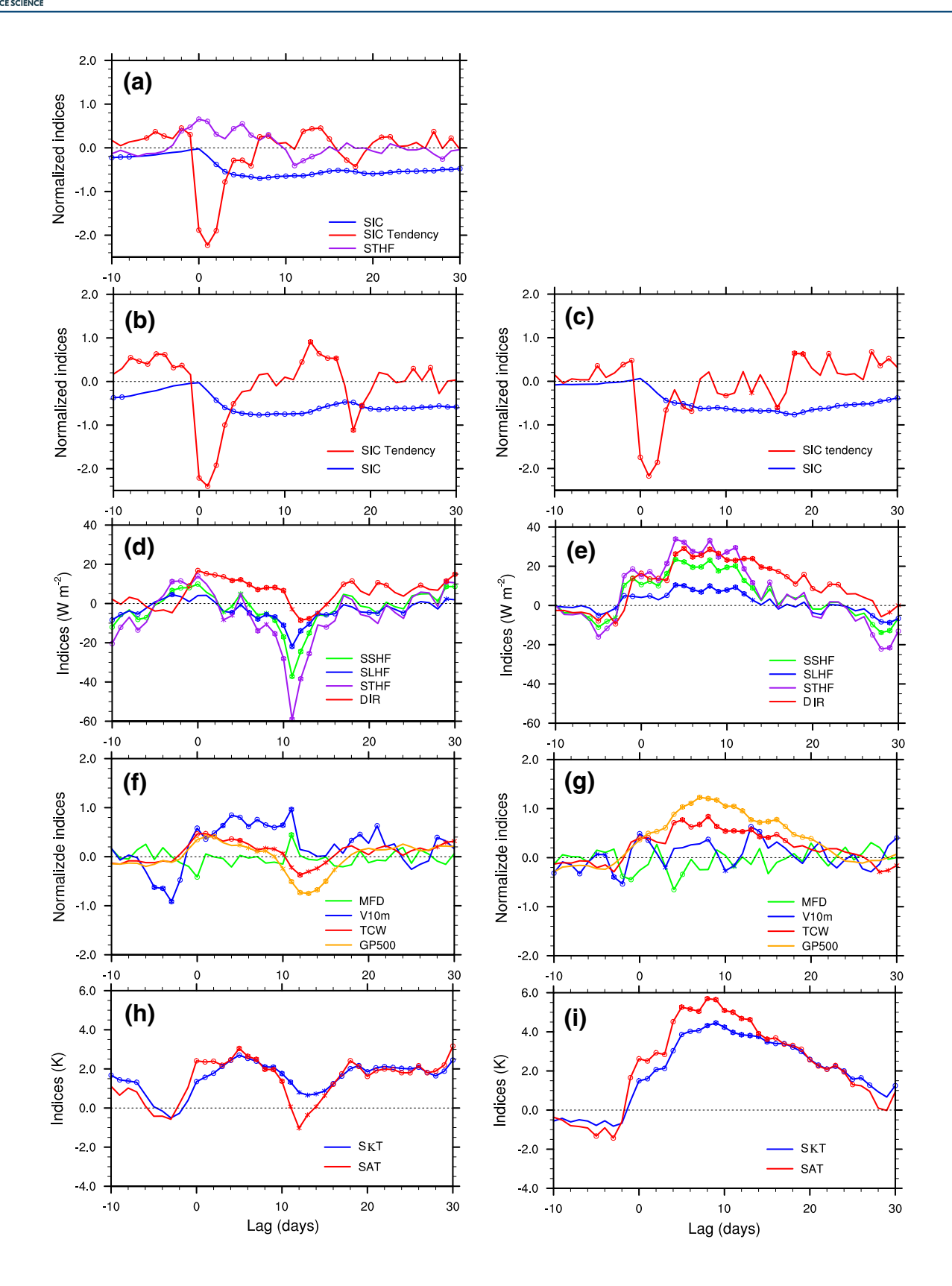
To further investigate the relationship between sea ice decline and the ASTHF, rapid sea ice decline events are divided into 3 bins, based on the value of the STHF index at lag +11 days (The upward and downward bins, or categories, are described in Section 1). Following this approach, 26 upward (25 downward) ASTHF events are identified based on BKS STHF index values at lag +11 days being less than -0.6 (greater than 0.1). The threshold value is different because the probability density function of the STHF index at lag +11 days is skewed (Figure 2), with a relatively weak upward ASTHF being most typical after rapid sea ice decline.

Lagged composites of all indices relative to the onset day for upward (downward) ASTHF events are shown in Figures 1b, 1d, 1f, and 1h (Figures 1c, 1e, 1g, and 1i). For the upward ASTHF events (Figure 1b), the largest negative sea ice tendency peaks at lag +1 day and has a magnitude a little greater than that for the downward ASTHF events (Figure 1c). The sea ice anomaly for the upward ASTHF events declines rapidly and reaches its minimum value at about lag +7 days and persists until at least lag +30 days. In contrast, the sea ice anomaly for the downward ASTHF events declines more gradually and reaches its minimum value at about lag +18 days.

The ASTHF shows marked differences between the two types of events (Figures 1d and 1e). For the upward ASTHF events, near lag 0 days when the sea ice decline is most rapid, the STHF index is positive (a downward ASTHF) and statistically significant. After lag +6 days, following most of the sea ice decline, the STHF index becomes negative (an upward ASTHF), reaching its minimum at lag +11 days and remaining statistically significant until lag +14 days. The SSHF index is stronger than the SLHF index, both of which follow the same general patterns as the STHF index (Figure 1d). For the downward ASTHF events, the STHF index is again positive (a downward ASTHF) near lag 0 days when the sea ice is declining most rapidly, with the ASTHF strengthening over the next several days, remaining large and downward until lag +15 days (Figure 1e).

The differences in the STHF, SLHF, and SSHF indices between the upward and downward categories are statistically significant from lag +4 to lag +13 days. Also, separate SSHF and SLHF indices are calculated for the open-water and ice-covered parts of the BKS. It is found that the open-water and ice-covered indices exhibit a similar evolution with time lag, for both the upward and downward ASTHF events, with the open-water indices exhibiting larger amplitudes than the ice-covered indices (not shown). In addition, even though the DIR index is mostly positive for both events at positive lags, compared to the upward ASTHF events, the DIR index for the downward ASTHF events is larger, and more persistent, with statistically significant

JIANG ET AL. 3 of 10



JIANG ET AL. 4 of 10

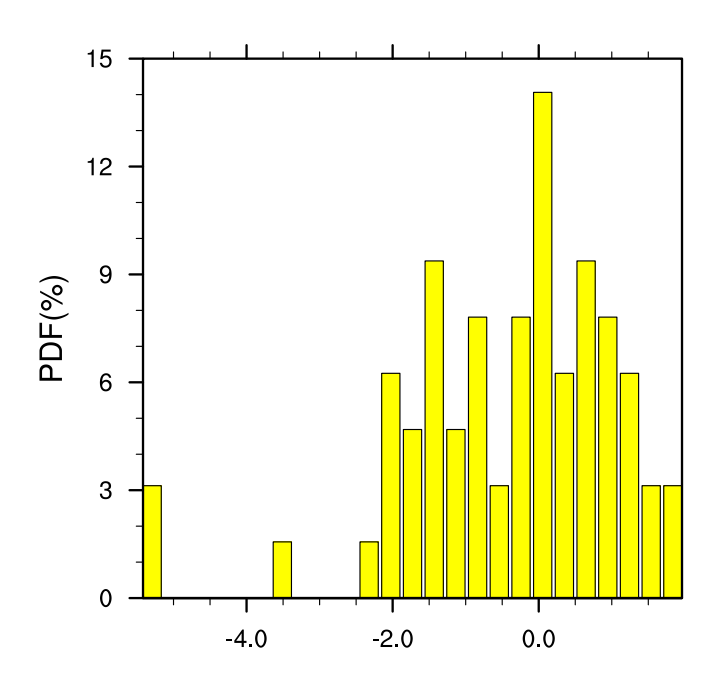


Figure 2. The probability density functions of the STHF index at lag +11 days for all events.

values for the difference being seen from lag +4 to lag +15 days (Note that the ECMWF sign convection is that surface DIR fluxes are positive).

There are marked differences in the TCW, MFD, and V10 m indices between the upward and downward ASTHF events (Figures 1f and 1g). The TCW index for both events has a similar temporal evolution as the DIR index, again being stronger and more persistent at positive lags for the downward ASTHF events. Furthermore, it is found that the moisture flux convergence (negative values for MFD) for the downward ASTHF events is also stronger and more persistent than that for the upward ASTHF events. Lastly, a comparison of V10 m shows that the wind near the surface for the upward ASTHF events is stronger and more persistent than that for the downward ASTHF events, with statistically significant positive values from lag 0 to lag +11 days for the upward ASTHF events.

The SAT and SKT indices also exhibit larger amplitudes and more persistence in the downward ASTHF events compared to those in the upward ASTHF events (Figures 1h and 1i). The most striking difference occurs near lag +11 days, where it can be seen that the difference between the SAT and SKT is negative for the upward ASTHF events and vice versa for the downward ASTHF events. This sign difference can explain the opposite direction of the anomalous SSHF between the two events at positive lags. In addition, at lag +11 days, the anomalous TCW is negative and the anomalous 10-m wind is positive for the upward ASTHF events, and vice versa for the downward ASTHF events, which can account for the oppo-

site direction of the anomalous SLHF for the two events. This relationship between SLHF and total column water is consistent with the local and external moisture sources proposed by Zhong et al. (2018).

3.2. Relative Importance of Atmospheric Thermal Processes Versus Wind-Driven Sea Ice Motion for Rapid Sea Ice Decline

To gain insight into the processes that determine the direction of the ASTHF that follows the sea ice loss, we will examine mechanisms which have been shown in previous studies to drive rapid sea ice decline. As we will see, the processes that drive sea ice loss are linked to the direction of the ASTHF following the decline in sea ice. We consider three mechanisms. These are (1) the decline of sea ice due to wind-driven sea ice motion (e.g., Deser et al., 2000; Fang & Wallace, 1994; Rigor et al., 2002; Sorteberg & Kvingedal, 2006), (2) the melting of sea ice due to enhanced DIR (e.g., D. H. Luo et al., 2016a, 2016b, 2017; D-S. R. Park et al., 2015; Francis & Hunter, 2006; H-S. Park, Lee, Kosaka, et al., 2015, H-S. Park, Lee, Son, et al., 2015; Gong & Luo, 2017; Zhong et al., 2018), and (3) the melting of sea ice arising from downward anomalous SSHF (Chen et al., 2018; Lee et al., 2017; Luo et al, 2017, 2019; Gong & Luo, 2017; Gong et al., 2017). The latter two processes are associated with the intrusion of warm, moist air that originates in midlatitudes which leads to an increase in DIR and SSHF (Chen et al., 2018; D-S. R. Park et al., 2015; Sorokina et al., 2016). If mechanism (1) dominates the driving of the sea ice decline, it would be expected that the ASTHF following the sea ice loss would be upward, whereas if mechanisms (2) and/or (3) dominate, a downward, rather than an upward, ASTHF may be expected following the loss of sea ice.

As can be seen in Figure 3, for the upward ASTHF events, there exists strong northeastward sea ice motion over the northeastern BKS with a maximum amplitude of about 6 cm s $^{-1}$ from lag 0 to +2 days, when the negative sea ice tendency is strongest. In contrast, for the downward ASTHF events, although there is still

Figure 1. Lagged composites of various indices based on the sea ice tendency index for (a) all events; (b, d, f, and h) upward anomalous surface turbulent heat flux (ASTHF) events; (c, e, g, and i) downward ASTHF events, which include sea ice concentration (SIC), SIC tendency, surface air temperature (SAT), surface skin temperature (SKT), 500 hPa geopotential height (GP500), 10-m wind speed (V10 m), total column water (TCW), surface downward infrared radiation (DIR), vertical integral of divergence of moisture flux (MFD), surface sensible heat flux (SSHF), surface latent heat flux (SLHF), and surface turbulent heat flux (STHF). The open circles indicate statistically significance (p < 0.05) using Monte Carlo bootstrapping, and the crosses indicate statistically significance (p < 0.05) of difference using Student's-t test.

JIANG ET AL. 5 of 10

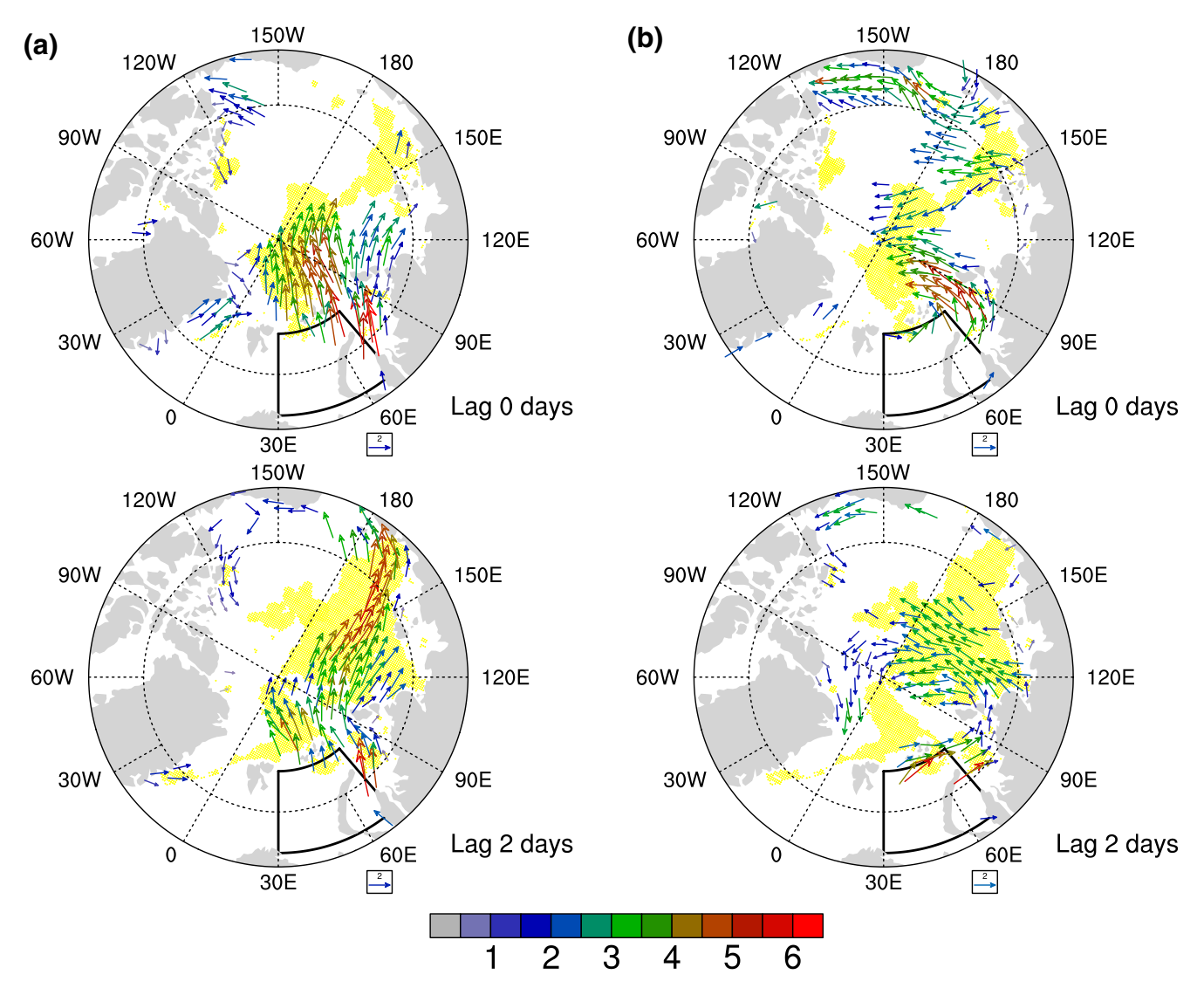


Figure 3. Lagged composites of the anomalous sea ice motion vectors (cm s⁻¹) for (a) upward anomalous surface turbulent heat flux (ASTHF) events and (b) downward ASTHF events. The vectors indicate statistically significance (p < 0.2), and the yellow shaded indicate statistically significance (p < 0.1) of difference using Student's-t test.

northeastward sea ice motion, its maximum amplitude over the BKS is smaller during the same time interval. These results support the view that wind-driven sea ice motion is indeed playing a more important role for the sea ice decline during upward ASTHF events.

To further examine the relative contributions by sea ice motion, DIR, and SSHF to sea ice decline, we estimate the cumulative changes in sea ice thickness due to these processes by following the method used in H-S. Park, Lee, Son, et al. (2015) wherein the impact of DIR was computed using the "toy model" of Eisenman (2012). We use the same model to estimate the impact of both anomalous DIR and SSHF. An implicit assumption in this calculation is that the processes that change sea ice thickness over the BKS also account for the decline in SIC. The time evolution of sea ice thickness change averaged over the BKS (Figure S1) during the time period of the largest sea ice decline, i.e., from lag 0 to +4 days, indicates that sea-ice motion, enhanced DIR and downward SSHF make similar contributions to the sea ice thickness decline for the downward ASTHF events. In contrast, for the upward ASTHF events, sea ice motion dominates, followed by a strengthened DIR, with the anomalous SSHF playing the smallest role. These results show that when

JIANG ET AL. 6 of 10



the loss of sea ice is due to wind-driven sea-ice motion, the ASTHFs that follow are upward, and when the sea ice decline is due to sea-ice motion, anomalous DIR and SSHF, the subsequent ASTHFs are downward.

3.3. Characteristics of the Atmospheric Circulation During the Rapid Sea Ice Decline Events

The results hitherto suggest that there is a difference in the atmospheric circulation beyond the BKS between the upward and downward ASTHF events. Figure 4a shows that the upward ASTHF events are associated with a westward propagating zonal wavenumber 1 disturbance at high latitudes, which includes a blocking high over northern Europe (B. H. Luo et al., 2019). Between lag -2 and lag +6 days, there is a wave train that extends from the subtropical western Pacific, across the North Pacific, southern Canada, and the northern United States, the North Atlantic, and the Norwegian Sea, toward the BKS. The location and direction of propagation of this wave train is most apparent from the wave activity flux vectors in Figure 4a (Takaya & Nakamura, 2001). The anomalous SLP pattern at high latitudes mirrors the anomalous 300-hPa streamfunction pattern (Figure S2a), indicating that the circulation pattern is barotropic. This barotropic structure suggests that the high latitude circulation is driven remotely.

The above wave train, for the upward ASTHF events, is found to be preceded by Madden Julian Oscillation (MJO)-like convection that corresponds to MJO phases 5–6, based on the Wheeler and Hendon (2004) RMM1 and RMM2 indices (these indices are statistically significant as far back as lag -8 days) (Figure S3a). Consistent with many studies which show that tropical convection can excite a poleward propagating Rossby wave train (Hoskins & Karoly, 1981), between lag -2 to lag 0 days, the upstream positive anomaly over the northeast Pacific weakens and the downstream negative anomaly over northern Canada amplifies (Figure 4a). At lag -2 days, a positive anomaly is centered over the BKS. This anomaly reaches its maximum amplitude at lag 0 days. The anomalous V10 m (Figure S4a) indicates that the direction and strength of the sea ice motion is consistent with the 10-m wind. The above sequence describes a linkage between tropical convection, a poleward propagating Rossby wave train, surface circulation anomalies induced by the upper tropospheric Rossby wave train, which in turn drive sea ice motion over the BKS.

For the downward ASTHF events (Figure 4b), between lags -4 and 0 days, a synoptic-scale wave train propagates across North America, the North Atlantic, toward the Ural Mountains and the southern BKS. This direction of propagation can also be seen in the wave activity flux vectors. At lag 0 days, a zonal wavenumber 1 disturbance develops poleward of 60° N. Throughout lags 2–6 days, the trough centered over Greenland propagates eastward and weakens, while the ridge centered over Kara Sea and northern Ural Mountains remains stationary and amplifies. The anomalous ridge closely resembles a Ural block. This ridge building, which is preceded by the upstream synoptic-scale wave train, also supports the perspective that the ridge is likely to be a Ural block (Luo, 2005a, 2005b).

The wave train for the downward ASTHF events is found to be preceded by MJO-like convection that corresponds to MJO phases 4–6 (these indices are statistically significant as far back as lag –20 days) (Figure S3b). Compared to the upward ASTHF events, the anomalous V10 m over the BKS are noticeably weaker in the downward ASTHF events during lag 0 days to lag 2 days (Figure S4b). Also, the moisture fluxes for the downward ASTHF events come from farther south over Norwegian Sea and western Europe, compared to the upward ASTHF events where the moisture fluxes come from west of the BKS and Greenland Sea (Figure S5). This difference likely accounts for the much warmer and moister air entering the Arctic in the downward ASTHF events. Consistently, for the downward ASTHF events, this long-lasting Ural block is favorable for the transport of warm, moist air into the BKS, as has been shown by Gong and Luo (2017), D. H. Luo et al. (2016a, 2016b) and Chen et al. (2018).

These features relating the circulation anomalies, SIC and STHF can be summarized by comparing the temporal evolution of the corresponding circulation indices. As can be seen in Figures 1f and 1g, for both events, the circulation anomalies GP500 (averaged over 40°–80°E, 55°–75°N, the domain with the key circulation anomaly at lag 0 days in Figure 4), are in phase with the sea ice tendency, implying that the circulation anomalies lead the SIC anomalies by a few days (Gong & Luo, 2017; D-S. R. Park et al., 2015), and the circulation anomalies lead the ASTHF by 10 days for the upward ASTHF events and by 6 days for the downward ASTHF events.

JIANG ET AL. 7 of 10

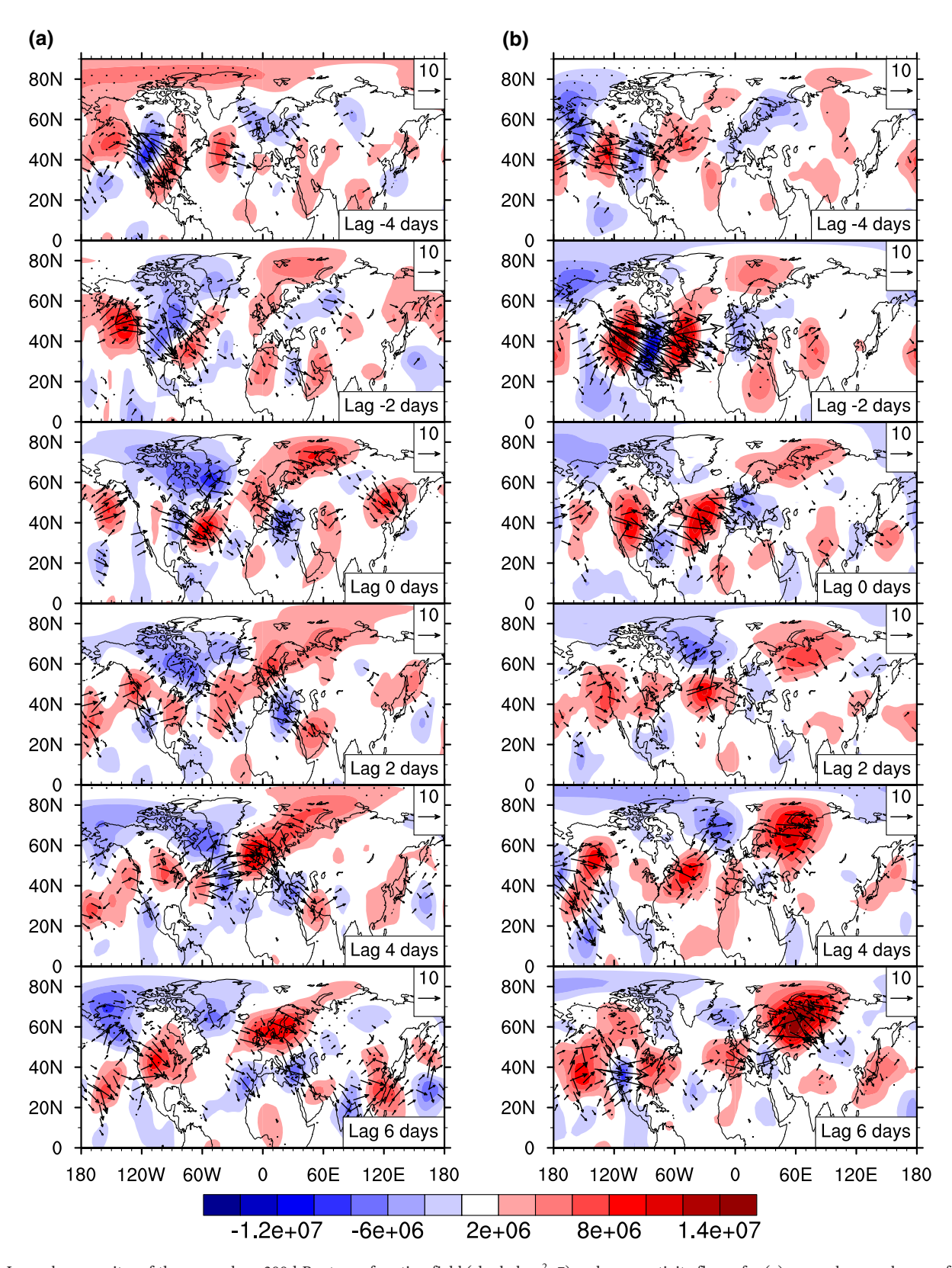


Figure 4. Lagged composites of the anomalous 300-hPa streamfunction field (shaded, $m^2 s^-$) and wave activity fluxes for (a) upward anomalous surface turbulent heat flux (ASTHF) events and (b) downward ASTHF events. The dots indicate statistically significance (p < 0.1) of streamfunction differences using Student's-t test.

JIANG ET AL. 8 of 10



4. Conclusions and Discussion

In this study, we have investigated atmospheric conditions before and after sea ice loss over the BKS for two types of events, distinguished by the sign of the ASTHF at lag +11 days, when the ASTHF averaged over all events is largest after the rapid sea ice decline. For the upward ASTHF events, the loss of sea ice has the potential to impact the atmosphere. In contrast, for the downward ASTHF events, the impact of sea ice loss on the atmosphere would be minimal. In the upward ASTHF events, the anomalous SAT is lower than the anomalous surface skin temperature, the surface wind is stronger and the air is drier, allowing for anomalous upward sensible and latent heat fluxes after the sea ice decline. For the downward ASTHF events, the anomalous SAT is higher than the anomalous skin temperature, and the air is relatively warm and humid, with weaker winds, resulting in anomalous downward surface sensible and latent heat fluxes after the loss of sea ice. In addition, statistically significant MJO index anomalies are found to precede both ASTHF events, and these are followed by upper tropospheric circulation anomalies that extend from low latitudes to the Arctic. These results suggest that direction of the ASTHF after the sea ice decline is linked to the circulation, temperature and moisture anomalies that are initially excited by the MJO. These results are insensitive to the threshold amplitude of the SIC tendency index (-0.5 instead of -1.0), persistence criterion (1 day instead of 3 days), and the time for categorizing the STHF index for the two types of events (average from lag +11 to +13 days instead of lag +11 days).

Finally, the results of this study raise a question on the common approach adopted in climate model studies in which the atmospheric response to sea ice loss is examined by prescribing a sea ice boundary condition that mimics the observed sea ice loss in the BKS (Deser et al., 2004, 2007; Honda et al., 2009; Peings & Magnusdottir, 2014). We show that only a subset of rapid sea ice decline events has the potential to influence the atmosphere on the intraseasonal time scale, since the anomalous STHF during these events can be either upward or downward. Therefore, when designing numerical model experiments to investigate the transient atmospheric response to sea ice loss, if observed SIC anomalies are to be prescribed, it would be best to use SIC anomalies only from those time periods when the anomalous STHF is upward. In doing so, it would be also important to use the corresponding atmospheric state, e.g., wind and temperature, as the initial condition.

Data Availability Statement

The authors acknowledge the European Centre for Medium-Range Weather Forecasts and the National Snow and Ice Data Center for providing the ERA-interim reanalysis data (http://apps.ecmwf.int/datasets/data/interim-full-daily/), daily sea ice motion data (https://nsidc.org/data/nsidc-0116) and sea ice thickness data (http://psc.apl.uw.edu/research/projects/arctic-sea-ice-volume-anomaly/data/), respectively.

Acknowledgments

This work is jointly supported by the National Natural Science Foundation of China (No. 41775001) and National Science Foundation grants OPP-1723832 and AGS-1822015.

References

Alexander, M. A., Bhatt, U. S., Walsh, J. E., & Michael, S. (2004). The atmospheric response to realistic Arctic sea ice anomalies in an AGCM during winter. *Journal of Climate*, 17(5), 890–905.

Blackport, R., Screen, J. A., van der Wiel, K., & Bintanja, R. (2019). Minimal influence of reduced Arctic sea ice on coincident cold winters in mid-latitudes. *Nature Climate Change*, 9, 697–704. https://doi.org/10.1038/s41558-019-0551-4

Cavalieri, D. J., Parkinson, C. L., Gloersen, P., & Zwally, H. (1996). Sea ice concentrations from Nimbus-7 SMMR and DMSPSSM/I-SSMIS passive microwave data (updated yearly). NASA DAAC at the National Snow and Ice Data Center.

Chen, X. D., Luo, D. H., Feldstein, S. B., & Lee, S. (2018). Impact of winter Ural blocking on Arctic sea ice: Short-time variability. *Journal of Climate*, 31, 2267–2282.

Dee, D. P., Uppala, S. M., Simmons, A. J., Berrisford, P., Poli, P., & Kobayashi, S. (2011). The ERA-Interim reanalysis: Configuration and performance of the data assimilation system. *Quarterly Journal of the Royal Meteorological Society*, 137(657), 553–597. https://doi.org/10.1002/gi.828

Deser, C., Magnusdottir, G., Saravanan, R., & Phillips, A. (2004). The effects of North Atlantic SST and sea-ice anomalies on the winter circulation in CCM3. Part II: Direct and indirect components of the response. *Journal of Climate*, 17(5), 877–889.

Deser, C., Tohas, R. A., & Peng, S. L. (2007). The transient atmospheric circulation response to North Atlantic SST and sea ice anomalies. *Journal of Climate*, 20, 4751–4767.

Deser, C., Walsh, J. E., & Timlin, M. S. (2000). Arctic sea ice variability in the context of recent atmospheric circulation trends. *Journal of Climate*, 13, 617–633.

Eisenman, I. (2012). Factors controlling the bifurcation structure of sea ice retreat. *Journal of Geophysical Research*, 117, D01111. https://doi.org/10.1029/2011JD016164

Fang, Z., & Wallace, J. M. (1994). Arctic sea ice variability on a timescale of weeks: Its relation to atmospheric forcing. *Journal of Climate*,

Francis, J. A., & Hunter, E. (2006). New insight into the disappearing Arctic sea ice. Eos, Transactions American Geophysical Union, 87, 509–511.

JIANG ET AL. 9 of 10

Geophysical Research Letters

- Gong, T. T., Feldstein, S. B., & Lee, S. (2017). The role of downward infrared radiation in the recent Arctic winter warming trends. *Journal of Climate*. 30, 4937–4949.
- Gong, T. T., Feldstein, S. B., & Lee, S. (2020). Rossby wave propagation from the Arctic into midlatitudes: Does it arise from in-situ latent heating or a trans-Arctic wave train? *Journal of Climate*, 33, 3619–3633.
- Gong, T. T., & Luo, D. H. (2017). Ural Blocking as an amplifier of the Arctic sea ice decline in winter. Journal of Climate, 30, 2639-2654.
- Honda, M., Inoue, J., & Yamane, S. (2009). Influence of low Arctic sea-ice minima on anomalously cold Eurasian winters. *Geophysical Research Letters*, 36, L08707, https://doi.org/10.1029/2008GL037079
- Honda, M., Yamazaki, K., Nakamura, H., & Kensuke, T. (1999). Dynamic and thermodynamic characteristics of atmospheric response to anomalous sea-ice extent in the sea of Okhotsk. *Journal of Climate*, 12(12), 3347–3358.
- Hoskins, B. J., & Karoly, D. (1981). The steady linear response of a spherical atmosphere to thermal and orographic forcing. *Journal of the Atmospheric Sciences*, 38, 1179–1196.
- Inoue, J., Hori, M. E., & Takaya, K. (2012). The role of Barents sea ice in the wintertime cyclone track and emergence of a warm-Arctic cold-Siberian anomaly. *Journal of Climate*, 25, 2561–2568.
- Jiang, Z. N., Feldstein, S. B., & Lee, S. (2017). The relationship between the Madden-Julian Oscillation and the North Atlantic Oscillation. Quarterly Journal of the Royal Meteorological Society, 143, 240–250.
- Kug, J.-S., Jeong, J.-H., Jang, Y.-S., Kim, B. M, Folland, C. K, & Son, S. W (2015). Two distinct influences of Arctic warming on cold winters over North America and East Asia. Nature Geoscience, 8, 759–763. https://doi.org/10.1038/NGEO2517
- Lee, S., Gong, T., Feldstein, S. B., Screen, J. A., & Simmonds, I. (2017). Revisiting the cause of the 1989–2009 Arctic surface warming using the surface energy budget: Downward infrared radiation dominates the surface fluxes. Geophysical Research Letters, 44, 10654–10661. https://doi.org/10.1002/2017GL075375
- Liptak, J., & Strong, C. (2014). The winter atmospheric response to sea ice anomalies in the Barents Sea. *Journal of Climate*, 27, 914–924. Luo, B. H., Luo, D. H., Wu, L. X., Zhong, L., & Simmonds, I. (2017). Atmospheric circulation patterns which promote winter Arctic sea ice decline. *Environmental Research Letters*, 12, 054017.
- Luo, B. H., Wu, L. X., Luo, D. H., & Ian, S. (2019). The winter midlatitude-Arctic interaction: effects of North Atlantic SST and high-latitude blocking on Arctic sea ice and Eurasian cooling. Climate Dynamics, 52, 2981–3004.
- Luo, D. H. (2005a). A barotropic envelope Rossby soliton model for block-eddy interaction. Part I: Effect of topography. Journal of the Atmospheric Sciences, 62(1), 5–21.
- Luo, D. H. (2005b). A barotropic envelope Rossby soliton model for block-eddy interaction. Part II: Role of westward-traveling planetary waves. Journal of the Atmospheric Sciences, 62(1), 22–40.
- Luo, D. H., Xiao, Y. Q., Yao, Y., Dai, A., Simmonds, I., & Franzke, C. L. E., (2016). Impact of Ural blocking on winter warm Arctic-cold Eurasian anomalies. Part I: Blocking-induced amplification. *Journal of Climate*, 29, 3925–3947.
- Luo, D. H., Xiao, Y. Q., Yao, Y., Dai, A., Simmonds, I., & Franzke, C. L. E., (2016). Impact of Ural blocking on winter warm Arctic-cold Eurasian anomalies. Part II: The link to the North Atlantic Oscillation. *Journal of Climate*, 29, 3949–3971.
- Magnusdottir, G., Deser, C., & Saravanan, R. (2014). The effects of North Atlantic SST and sea ice anomalies on the winter circulation in CCM3. Part I: Main features and storm track characteristics of the response. *Journal of Climate*, 17, 857–876.
- Park, D.-S. R., Lee, S. Y., & Feldstein, S. B. (2015). Attribution of the recent winter sea ice decline over the Atlantic sector of the Arctic ocean. *Journal of Climate*, 28, 4027–4033.
- Park, H.-S., Lee, S., Kosaka, Y., Son, S.-W., & Kim, S.-W. (2015). The impact of Arctic winter infrared radiation on early summer sea ice. Journal of Climate. 28. 6281–6296.
- Park, H.-S., Lee, S., Son, S. W., Feldstein, S. B., & Kosaka, Y. (2015). The impact of poleward moisture and sensible heat flux on Arctic winter sea ice variability. *Journal of Climate*, 28, 5030–5040.
- Peings, Y., & Magnusdottir, G. (2014). Response of the wintertime Northern Hemisphere atmospheric circulation to current and projected Arctic Sea ice decline: A numerical study with CAM5. *Journal of Climate*, 27(1), 244–264.
- Perlwitz, J., Hoerling, M., & Dole, R. (2015). Arctic tropospheric warming: Causes and linkages to lower latitudes. *Journal of Climate*, 28, 2154–2167.
- Petoukhov, V., & Semenov, V. A. (2010). A link between reduced Barents-Kara sea ice and cold winter extremes over northern continents[J]. *Journal of Geophysical Research*, 115(D21), D21111. https://doi.org/10.1029/2009JD013568
- Rigor, I. G., Wallace, J. M., & Colony, R. L. (2002). Response of sea ice to the Arctic Oscillation. Journal of Climate, 15, 2648-2663.
- Rinke, A., Maslowski, W., Dethloff, K., & Clement, J. (2006). Influence of sea ice on the atmosphere: A study with an arctic atmospheric regional climate model. *Journal of Geophysical Research*, 111, D16103. https://doi.org/10.1029/2005JD006957
- Screen, J. A., Deser, C., & Simmonds, I. (2012). Local and remote controls on observed Arctic warming. *Geophysical Research Letters*, 39, L10709. https://doi.org/10.1029/2012GL051598
- Sorokina, S. A., Li, C., Wettstein, J. J., & KvamstØ, N. G. (2016). Observed atmospheric coupling between Barents sea ice and the warm-Arctic cold-Siberian anomaly pattern. *Journal of Climate*, 29, 495–511.
- Sorteberg, A., & Kvingedal, B. (2006). Atmospheric forcing on the Barents Sea winter ice extent. *Journal of Climate*, 19, 4772–4784. https://doi.org/10.1175/JCLI3885.1
- Takaya, K., & Nakamura, H. (2001). A formulation of a phase-independent wave-activity flux for stationary and migratory quasigeostrophic eddies on a zonally varying basic flow. *Journal of the Atmospheric Sciences*, 58, 608–627.
- Tschudi, M., Meier, W. N., Stewart, J. S., Fowler, C., & Maslanik, J. (2019). Polar pathfinder daily 25 km EASE-Grid sea ice motion vectors (Version 4, Indicate subset used) Boulder, CO: NASA National Snow and Ice Data Center Distributed Active Archive Center. https://doi.org/10.5067/INAWUW070H7B
- Tyrlis, E., Bader, J., Manzini, E., Ukita, J., & Nakumura, H., (2020). On the role of Ural blocking in driving the warm Arctic-cold Siberia pattern. *Ouarterly Journal of the Royal Meteorological Society*, 146, 2138–2153.
- Wheeler, M. C., & Hendon, H. H. (2004). An all-season real-time multivariate MJO index: Development of an index for monitoring and prediction. *Monthly Weather Review*, 132, 1917–1932.
- Woods, C., & Caballero, R. (2016). The role of moist intrusions in winter Arctic warming and sea ice decline. *Journal of Climate*, 29, 4473–4485.
- Zhang, J., & Rothrock, D. A. (2003). Modeling global sea ice with a thickness and enthalpy distribution model in generalized curvilinear coordinates. *Monthly Weather Review*, 131, 845–861.
- Zhong, L. H., Hua, L. J., & Luo, D. H. (2018). Local and external moisture sources for the Arctic warming over the Barents-Kara Seas. Journal of Climate, 31, 1963–1982.

JIANG ET AL. 10 of 10